Available online at www.sciencedirect.com
SCIENCE DIRECT®
ELSEVIER
Nuclear Instruments and Methods in Physics Research A 528 (2004) 763–775
NUCLEAR INSTRUMENTS & METHODS IN PHYSICS RESEARCH Section A
www.elsevier.com/locate/nima

MCP-PMT timing property for single photons

M. Akatsu, Y. Enari, K. Hayasaka, T. Hokuue, T. Iijima, K. Inami*, K. Itoh, Y. Kawakami, N. Kishimoto, T. Kubota, M. Kojima, Y. Kozakai, Y. Kuriyama, T. Matsuishi, Y. Miyabayashi, T. Ohshima, N. Sato, K. Senyo, A. Sugi, S. Tokuda, M. Tomita, H. Yanase, S. Yoshino

Department of Physics, High Energy Physics Laboratory, Nagoya University, Furo-Cho, Chikusa, Nagoya 464-8602, Japan

Received 8 January 2004; received in revised form 1 April 2004; accepted 2 April 2004

Abstract

We have measured the performance, especially the timing properties, of micro-channel plate photo-multiplier tubes (MCP-PMTs) by irradiating with single photons with/without a magnetic field. A time resolution of $\sigma = 30$–35 ps was obtained for single photons under 1.5 T. With an MCP-PMT, a small time-of-flight counter, by means of Cherenkov light radiation instead of scintillation light has been prepared, and a time resolution $\sigma \sim 10$ ps was attained for a high-energy π-beam by multiple photons.

PACS: 85.60.Ha; 29.40.Ka; 42.70.Ce

Keywords: MCP; TTS; Single photon

1. Introduction

The micro-channel plate photo-multiplier tube (MCP-PMT) [1] provides several promising features for a high-energy particle-detection device; its operational ability to provide a very good time resolution under a strong magnetic field is definitely an advantageous factor. However, the detailed performance of the timing property for single or a few multiple photons, especially under a magnetic field, has not been adequately addressed thus far. We present here our results on this issue.

We have been developing a new type of Cherenkov ring imaging detector, a time-of-propagation (TOP) counter [2], as a possible next-generation particle-identification device at the KEKB-factory Belle experiment. The required performance of the photon detector is to be position sensitive and single-photon sensitive with a transit time spread (TTS) of $\sigma_{\mathrm{TTS}} < 100$ ps under a magnetic field of $B = 1.5$ T. Our recent study, furthermore, devised a simpler version of the TOP-counter [3] which, however, demands a better time resolution, say $\sigma_{\mathrm{TTS}} < 50$ ps. We have inspected

*Corresponding author. Tel.: +52-789-2902; fax: +52-782-5752.

E-mail address: kenji@hepl.phys.nagoya-u.ac.jp (K. Inami).

0168-9002/$ - see front matter © 2004 Elsevier B.V. All rights reserved.
doi:10.1016/j.nima.2004.04.207

Table 1
Characteristics of four MCP-PMTs

MCP-PMT	HPK6	BINP10	HPK10	Burle25
Size of PMT (mm)	45^{ϕ}	30.5^{ϕ}	52^{ϕ}	71×71[a]
Effective size (mm)	11^{ϕ}	18^{ϕ}	25^{ϕ}	50×50[b]
Photocathode	multialkali	multialkali	multialkali	bialkali
Distances (mm)	2.1/0.03/1.0	0.2/0.09/1.2	1.1/0.03/0.94	6.1/0/5.2
D[c] (μm)	6	10	10	25
$\alpha = L/D$[c]	40	40	43	40
Bias angle (deg)	13	5	12	10
Max. voltage (kV)	3.6	3.2	3.6	2.5
Divider ratio	2:4:1	3.4:30:1	2:4:1	1:10:1
Gain	2×10^6	$\sim 10^6$	$\sim 10^5$	6×10^5

All MCP-PMTs are of two-stage type; HPK6, BINP10, and HPK10 are of the single-anode type and Burle25 is the 2×2 multi-anode type. The fourth raw indicates the distance from the photocathode to MCP, the distance between two MCP plates, and the distance from the MCP to anode.

[a] An area of MCP-PMT in mm^2.

[b] An area of effective size in mm^2.

[c] D and L are the diameter and length of the MCP plate, respectively, and $\alpha = L/D$.

four different types of MCP-PMTs by irradiating with single photons or a few multiple photons with/without a B-field. Also, as a test for the practical use of an MCP-PMT, a small time-of-flight (TOF) counter by means of Cherenkov light radiation was prepared and beam tested; $\sigma \sim 10$ ps was obtained.

The MCP-PMTs tested here were Hamamatsu (HPK) 3809U-50-11X, BINP-mcp,[1] HPK 3809U-50-25X, and Burle 85001-501, which are hereafter abbreviated as HPK6, BINP10, HPK10, and Burle25, respectively, where the number indicates the diameter of the micro-channels. The characteristics of the four MCP-PMTs are listed in Table 1. All MCP-PMTs are of two-stage type. The HPK6, BINP10 and HPK10 are of the single-anode type, and the Burle25 is of the 2×2 multi-anode type.

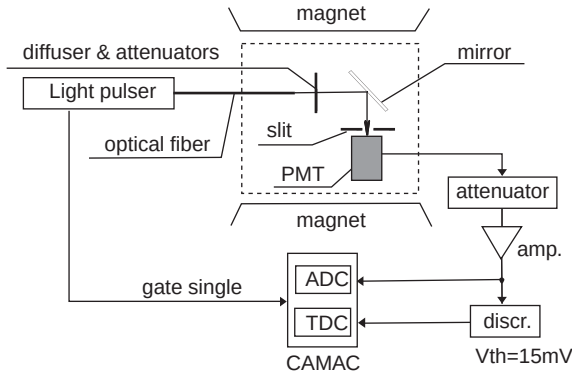

Fig. 1. Setup. See the text for a description.

2. Performances

2.1. Setup

The experimental setup used in this work is shown in Fig. 1. The light source, a Hamamatsu picosec light-pulser (PLP-02-SLDH-041), provides light with a wavelength of 405 ± 10 nm, a pulse width of 34 ps with a jitter of less than ± 10 ps, and a light spread of less than 2°. The output light, pulsed at a 1 kHz repetition rate, is guided by an optical fiber of 2 mmϕ and 2 m-long through a diffuser and attenuators, and reflected by a mirror to hit perpendicularly the MCP-PMT. To turn the axis of the MCP-PMT from the B-field direction the subsystem indicated by the dotted box in the figure is rotated.

The anode signal of the MCP-PMT is fed into an HPK amplifier (C5594: gain = 36 dB and

[1] MCP-PMT especially made to order by Ekran-FEP Ltd. for Budker Institute of Nuclear Physics.

frequency band = 50 kHz–1.5 GHz) through an attenuator; the output charge and the timing are measured by the ADC (0.25 pC/count) and TDC (25 ps/count) CAMAC modules, respectively. The threshold of the discriminator (Phillips Scientific, model 708) is optimized for the time resolution. It is 15 mV, about $\frac{1}{10}$ of the signal pulse heights, at most of the measurements.

2.2. Pulse shape

Fig. 2 shows the output pulses from the MCP-PMTs for single-photon irradiation under no B-field. HPK6 exhibits sharp and symmetrical shapes with a rise time of 300 ps and a pulse duration of $\sim$1 ns, while BINP10 shows a broad trapezoidal signal over a 4 ns time duration, followed by a relatively large undershoot. However, the signal rise is sharp, similar to that of the HPK6. We discuss BINP10's pulse shape in the last section.

2.3. ADC spectrum and PMT gain

The ADC distributions for single-photon irradiation are shown in Fig. 3 under $B = 0$ (thick histogram) and 1.5 T (dark histogram), while the open histogram centering at the 100th ADC channel is the pedestal distribution. The effect of the B-field appears either in a reduction of the gain (G), notably at HPK10 and Burle25, or in a compression of the ADC spectrum, while keeping the gain unchanged, as observed at HPK6 and BINP10. The latter fact might be attributed mainly to gain saturation. As a consequence of $B = 1.5$ T, the root mean square (rms) of the dominant part of the ADC distributions decreases roughly from 60% to 35% for HPK6, from 60% to 30% for BINP10, and from 70% to 60% for HPK10, but for Burle25 it increases from 50% to 60%. Due to this resolution improvement the two photo-electrons

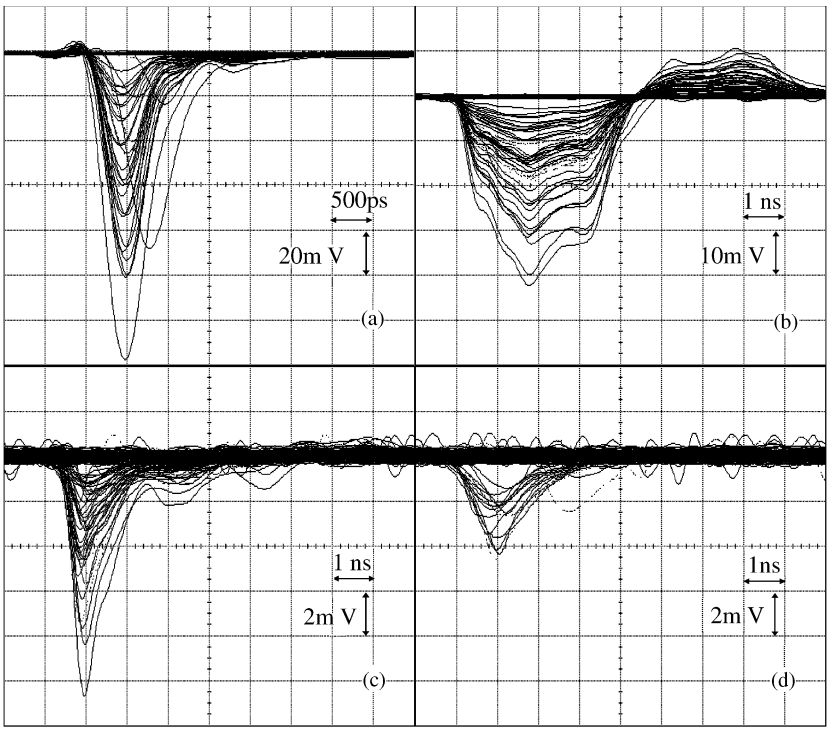

Fig. 2. MCP-PMTs output signals for single-photon irradiation under no B-field. (a) HPK6 (HV = 3.6 kV), (b) BINP10 (3.2 kV), (c) HPK10 (3.6 kV), and Burle25 (2.5 kV). A digital oscilloscope (Hewlett Packard, Infinium) with a frequency band of 1.5 GHz is used with a 50 Ω SMA cables in these measurements.

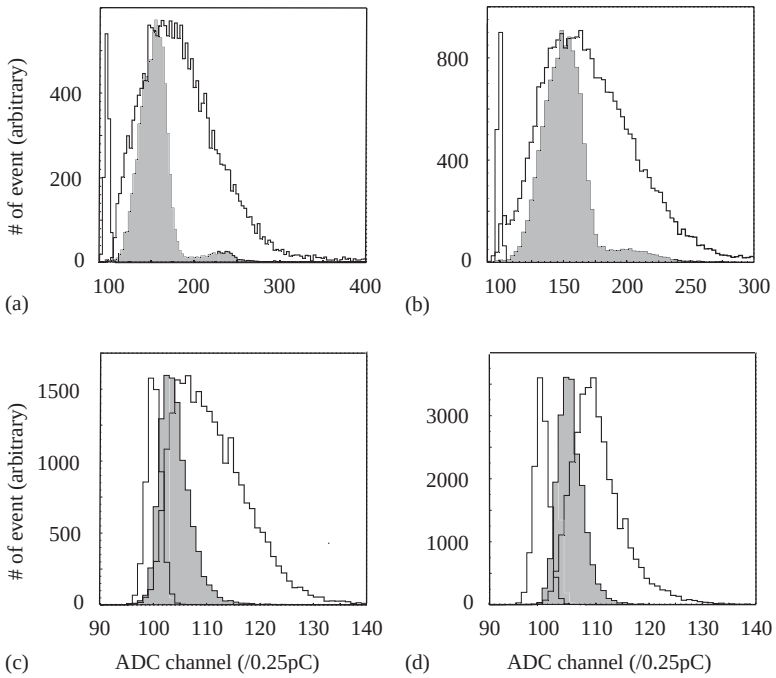

Fig. 3. ADC spectra of (a) HPK6, (b) BINP10, (c) HPK10, and (d) Burle25 for single-photon irradiation. The thick and dark histograms are spectra with $B = 0$ and 1.5 T, respectively, except for Burle25 it is with $B = 0.8$ T. The open histogram centering at the 100th ADC channel is the pedestal distribution. The applied HV is the same for both conditions without and with a B-field.

peak is well distinguished, as can be seen at HPK6 and BINP10.

From the ADC peak channel for single photoelectrons, we evaluated G as a function of HV under different B-field strengths (see, Fig. 4). HPK6 and BINP10 provided gains at the 10^6 level and did not exhibit a strong influence of the B-field, while HPK10 and Burle25 had $G \sim 5 \times 10^5$ at best. The achieved maximum gain was $G \simeq 3 \times 10^6$ for both HPK6 (HV = 3.6 kV) and BINP10 (3.2 kV), and 2×10^5 for HPK10 (3.6 kV) under $B = 1.5$ T, and 2×10^5 for Burle25 (2.5 kV) under 0.8 T. Burle25 could not be operational at a higher HV and B-field than that indicated in Fig. 4(a). G shows a somewhat B dependence, as can be seen in Fig. 4(b). While HPK6 and BINP10 exhibit almost a null and tiny dependence, respectively, HPK10 and Burle25 have their small maximum around $B \sim 0.2$–0.4 T.

2.4. ADC vs. TDC

Fig. 5 shows ADC vs. TDC scatter plots for single-photon irradiation under the same conditions as mentioned in Fig. 3 with no B-field. In order to avoid a timewalk correction, data are sliced into many narrow ADC regions and their time resolutions (σ_{sliced}) of individual regions are evaluated, as indicated by the open circles in the lower figures. Also plotted by closed circles are the same σ_{sliced}, but under $B = 1.5$ T (0.8 T for Burle25). The time resolution denoted by the term σ is the rms of a Gaussian function which well reproduces the dominant part of the observed TDC distributions. Fig. 6 shows ADC-sliced time distributions, for instance, at the ADC peak amplitude of the single photons for four MCP-PMTs.

It is found for all MCP-PMTs that as long as the pulse heights are the same, σ_{sliced} has the same

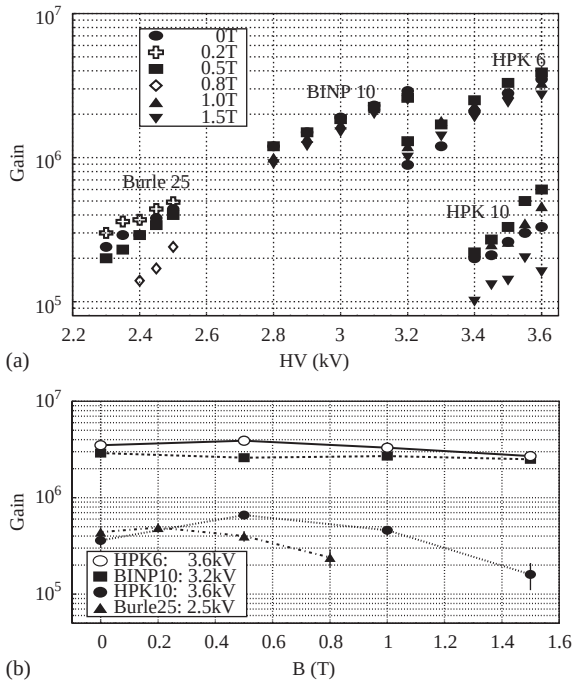

Fig. 4. (a) HV vs. G under different B-field strengths, and (b) B vs. G.

resolution, irrespective of the B-field strength. HPK6 and BINP10 both attain $\sigma_{\text{sliced}} \simeq 30$ ps at the single photo-electron ADC peak under $B = 0$ and 1.5 T. On the other hand, HPK10 and Burle25 reach $\sigma_{\text{sliced}} \simeq 40$ and 60 ps, respectively, under $B = 0$ T, while they are ~ 100 and 125 ps under $B = 1.5$ T because the G drop reduces their ADC peak channels. With a three-times higher gain, they are expected to attain $\sigma_{\text{sliced}} \simeq 30$ and 50 ps, respectively.

The time resolution (σ_{TTS}) for single-photon irradiation is obtained as a function of the B-field by applying a timewalk correction over the whole ADC region (see, Fig. 7). HPK6 and BINP10 show a stable σ_{TTS} of 30 and 35 ps, respectively, over wide B ranges from 0 to 1.5 T and HV = 2.8 to 3.2 kV (not indicated in Fig. 7). HPK10 and Burle25 exhibit, on the other hand, a strong dependence on the B-field and HV, and the $\sigma_{\text{TTS}} \sim 60$ and 100 ps, respectively, under $B = 1.5$ and 0.8 T with the maximum applicable HV.

2.5. Collection efficiency

The collection efficiency (CE) of secondary electrons is measured by comparing the count rate of the MCP-PMTs to that of our standard photomultiplier tube. The standard tube is the Hamamatsu H3171-04 LA9806, which has QE $\times$ CE = 0.1956 at $\lambda = 394$ nm, where QE is the quantum efficiency of the photocathode. The observed CE values under $B = 0$ T are listed in Table 2 together with QE; CE is stable within a 2% variation over $B = 0$–1.5 T.

BINP10 shows the highest CE value of 45% with a relatively lower QE than the others. It could be due to non-furnishing of a thin aluminum film at the MCP surface for ion feedback prevention. HPK6 and HPK10, on the other hand, are equipped with a film, which resultantly interferes with the photo-electron to yield the secondaries. The permeability of these Al films is expected to be around 50–60%.

2.6. Effect of the tilt to the magnetic field

The angle (ϕ) of the MCP-PMT axis relative to the B-field was varied and its effects on G and σ_{TTS} were measured. The tilted direction is defined so that the angle (ϕ_{ch}) between the micro-channel axis and B-field is $\phi_{\text{ch}} = \phi$-(bias angle). Figs. 8(a) and (b) show the ADC spectra with different ϕ angles for HPK6 and BINP10 under $B = 1.5$ T, respectively, and Fig. 9 shows the G vs. B and σ_{TTS} vs. B behaviors with different ϕ angles for all four types of MCP-PMTs. A similar behavior among G, B and ϕ can found in Ref. [4].

HPK6 demonstrates the highest G and sharpest ADC distribution at $\phi = 45^\circ$, while BINP10 does so at $\phi = 15^\circ$. Nevertheless, σ_{TTS} in the case of HPK6 does not depend on ϕ at all. On the other side, BINP10 indicates some σ_{TTS} variations following the G change at different ϕ angles. The tilted angle ϕ then affects the relation between σ_{TTS} and G. As an example, the relation of BINP10 is plotted in Fig. 10; ϕ affects G while keeping the σ_{TTS} vs. G relational form unchanged. The optimal ϕ angle for σ_{TTS} is 0° for BINP10 and any angle between 0° and 60° for HPK6.

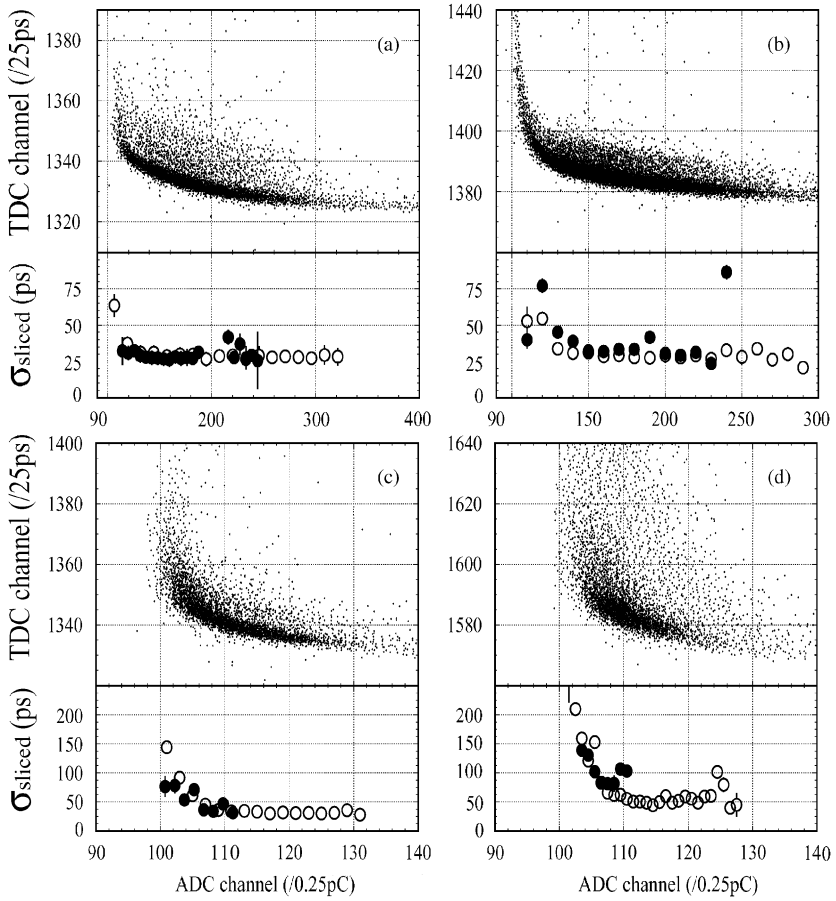

Fig. 5. Each upper figure shows ADC vs. TDC scatter plots for single-photon irradiation under no B-field with the same condition as in Fig. 3. The lower figures plot the ADC-sliced time resolution (σ_{sliced}) under $B = 0$ (open circles) and $B = 1.5$ T (0.8 T for Burle25) (closed circles). (a) HKP6, (b) BINP10, (c) HPK10, and (d) Burle25.

2.7. Multi-photon irradiation

For multi-photon irradiation, the ADC distributions are measured under a B-field (see, Fig. 11). HPK6 shows up to four photo-electron peaks under $B = 1.5$ T at $\phi = 0^\circ$, but does not under $B = 0$. BINP10 and Burle25 do not exhibit a multi-photo-electron structure under both $B = 0$ and 1.5 T at $\phi = 0^\circ$. However, when a finite ϕ angle is provided, BINP10 clearly shows multi photo-electron peaks at $B = 1.5$ T, but Burle25 does not. (HPK10 was not tested.)

3. A TOF counter with Cherenkov light

Since the decay-time constant of plastic scintillators, say 2–3 ns, is much larger than the above reported MCP-PMTs time resolution, σ_{TTS}, for single photons, the usage of such a fast MCP-PMT photo-device for a scintillator does not give full scope to its ability for TOF measurements. In other words, the photon radiator should have a similar, or faster, time response to that of the MCP-PMT: The Cherenkov radiation would fulfill such a demand, and a certain specifically designed

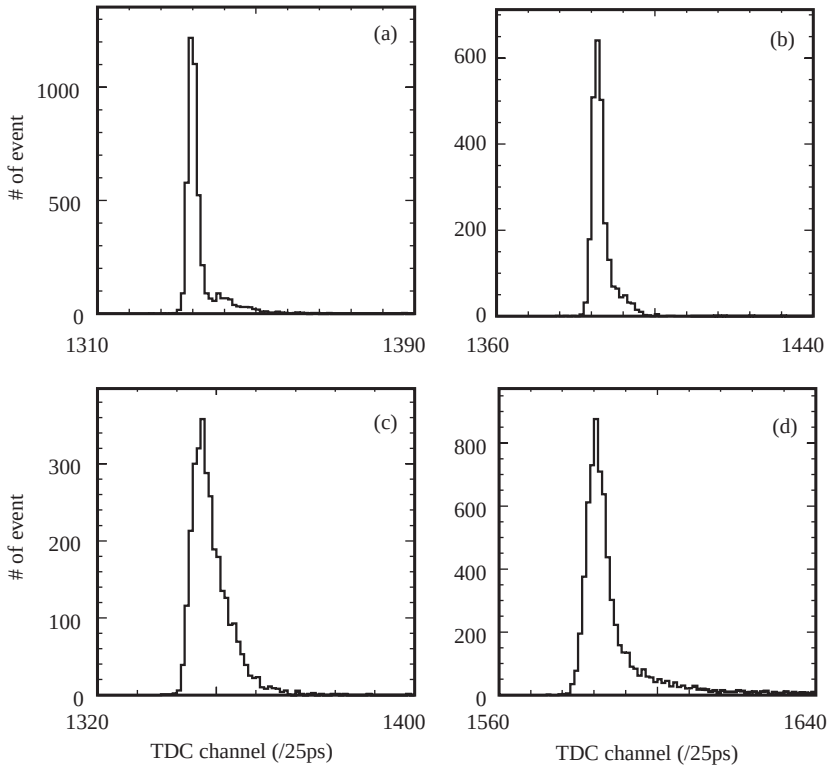

Fig. 6. ADC-sliced time distributions at the ADC peak amplitude for the single-photon irradiation under no *B*-field. Data are of those used in Fig. 5. The full scale of the horizontal axis is taken to be the same, 80 channels, for the four sub-figures. (a) HPK6, (b) BINP10, (c) HPK10, and (d) Burle25.

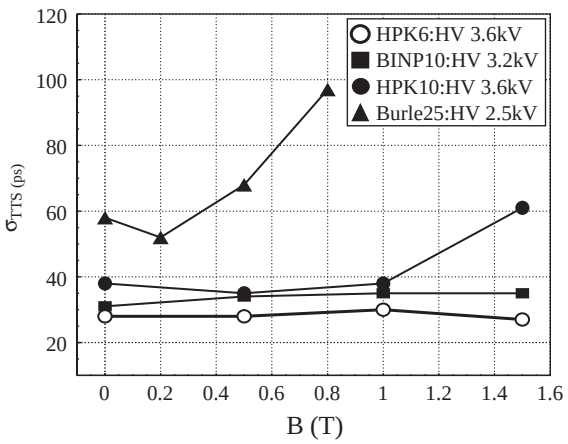

Fig. 7. The time resolutions for single-photon irradiation as a function of the *B*-fields. The applied HV is the same with that in Fig. 3.

Table 2
Measured collection efficiencies (CE). Quantum efficiency (QE) is evaluated at 405 nm by the respective companies

MCP-PMT	CE (%)	QE (%)	η (%)	Al film
HPK6	38	26	60	Yes
BINP10	45	18		No
HPK10	29	26	60	Yes
Burle25	29	24	30	No

The second right column is the open area ratio (η), and the first one indicates the existence of a coated aluminum thin film on the MCP surface for preventing ion feed-back. The applied HV is 3.6, 3.2, 3.6 and 2.5 kV at HPK6, BINP10, HPK10, and Burle25, respectively.

counter reported below also provides a sufficient number of photons to attain a high time resolution (σ_t), say 10 ps, in terms of photon statistics.

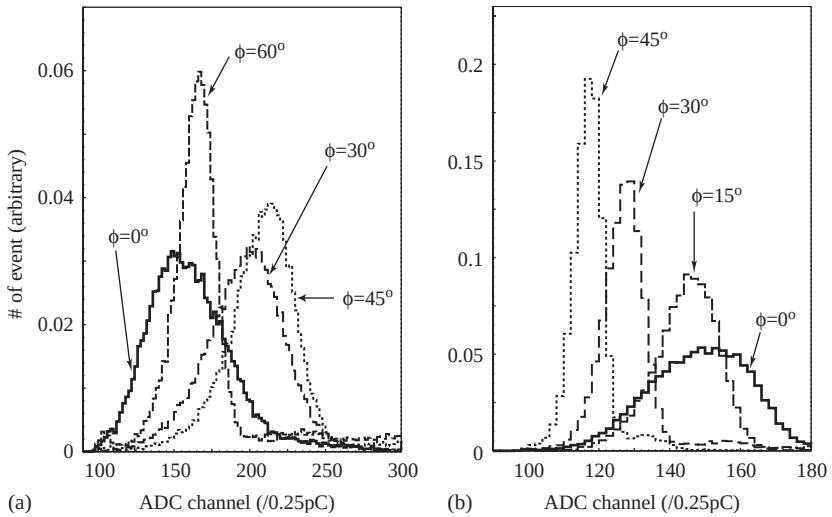

Fig. 8. ADC spectra with different ϕ angles under $B = 1.5$ T. (a) HPK6 and (b) BINP10.

3.1. The TOF counter

Quartz with a size of 16 mm × 16 mm × 40 mm^L is employed as a radiator, on one end of which a HPK10 is mounted and its other five side surfaces are aluminum coated by vacuum evaporation. This counter is expected to be used as a kind of tile TOF device along which axis particles pass through, as illustrated in Fig. 12. When the axis of the Cherenkov cone is nearly parallel to the counter axis, all light would arrive to the MCP-PMT within a narrow time duration. The chromaticity does not affect the light arrival time, because of its short propagation length.

We performed a beam test without a magnetic field at the KEK 12-GeV Proton Synchrotron using 3 GeV/c pion beams. The system is composed of two identical test counters, and two small scintillation counters for triggering and beam defining. The upstream test counter has a bit better detection efficiency than the downstream one, and they are separated by 30 cm.

3.2. Timing property of MCP-PMT alone

First test was performed without a quartz counter but using a 4 mm thick quartz window of HPK10 as a radiator, about 380 Cherenkov photons are expected to be produced over 200–900 nm of wavelength range, and about 24 photo-electrons to be then detected. A time resolution of $\sigma_t \simeq 16$ ps is expected by taking into account the timing uncertainty of the data-recording electronics system, $\sigma_{circuit} \sim 8$–9 ps. Without equipping the quartz radiator, we place the two HPK10s on the beam line and measure the ADC and TDC information.

Fig. 13(a) shows the output signal of a HPK10 with HV = 3.4 kV for a 3 GeV/c pion beam. The detected number of photo-electrons is evaluated from the ADC distributions by comparing to those for the light pulser. It results in ~ 50 photo-electrons, two-times larger than the expected value. The difference might be attributed to secondary electron production by the beam off the very front end of the MCP plate, itself.

Fig. 13(b) is a time-difference (tof) distribution between two HPK10s. By dividing the measured time-difference resolution (σ_{tof}) by $\sqrt{2}$ due to the same performance of two devices, the resultant time resolution for the single MCP-PMT is obtained as $\sigma_t = 13.6 \pm 0.1$ ps, which agrees well with the expectation.

3.3. Timing property of a test TOF counter

With equipping the quartz radiator, the numbers of photo-electrons are measured as ~ 260 and ~ 190 by the upstream and downstream counters,

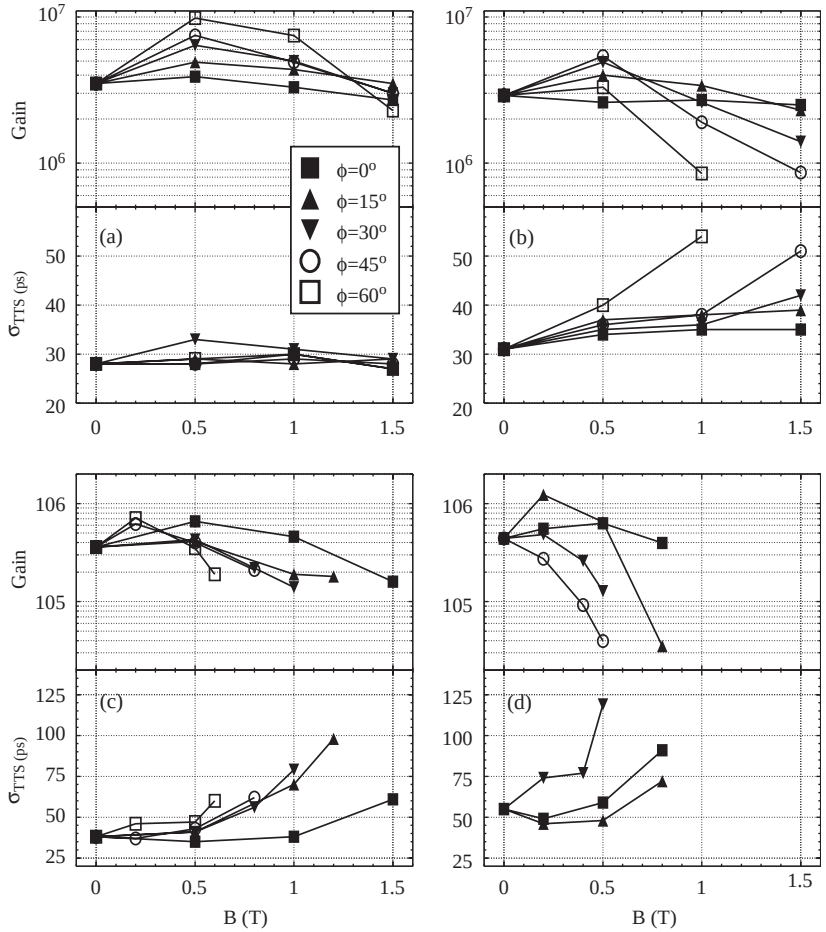

Fig. 9. Each upper figure shows the B vs. G relation and the lower one the B vs. σ_{TTS} relation with different ϕ angles for (a) HPK6, (b) BINP10, (c) HPK10, and (d) Burle25.

respectively, among which $\sim$210 and $\sim$140 are evaluated to be from the quartz radiator, which agree with the expectation. The difference in the numbers between the counters is due to their different detection efficiencies.

The time resolution is found to be $\sigma_t = 10.6 \pm 0.1$ ps for a single counter (Fig. 13(c)), where the uncertainty of the electronics system predominates this resolution.

4. Discussion and summary

The G vs. HV characteristic is often expressed, as below, based on a simple supposition that the total number of secondary electrons, or G, is the secondary emission factor ($\delta(V)$) powered by the number of collisions ($n(V)$) for multiplication and the electrons are perpendicularly emitted from the MCP wall with a kinetic energy of eV_0:

$$G = \delta(V)^{n(V)} = \left(\frac{KV}{\kappa}\right)^{\kappa}, \quad \kappa = \frac{4V_0\alpha^2}{V}, \tag{1}$$

where V is the applied HV over the MCP plates and $\delta(V) = KV_c$ with an electron collision energy of eV_c and coefficient K [5]. This relation under a magnetic field can be expressed in a similar way as

$$G = \left(\frac{KV}{\kappa}\right)^{\kappa \cos^2 \phi}, \quad \kappa = \frac{e}{2m_e}\frac{L^2}{V}\left(\frac{B}{\theta}\right)^2, \tag{2}$$

where θ is an angle that the emitted electron is turned during its flight by the B-field: $\cos\theta = \rho/\sqrt{\rho^2 + (D/2)^2}$, and ρ is the electron's Lamor radius. The tilted angle (ϕ) is briefly considered to shorten the MCP channel length by a factor of $\cos\phi$ for $n(V)$, but not $\delta(V)$.

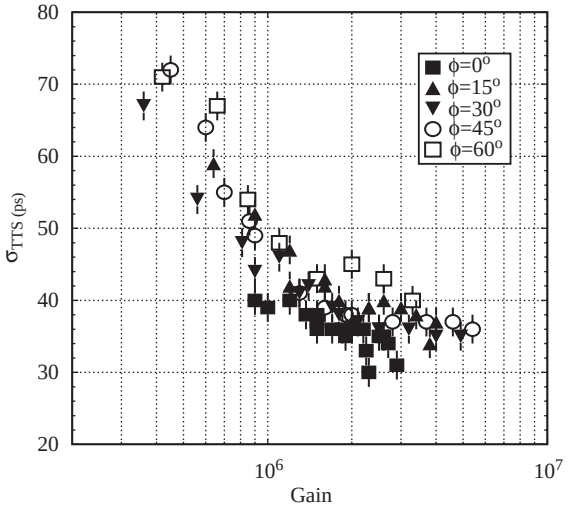

Fig. 10. G vs. σ_{TTS} for BINP10 with different ϕ angles.

Although these simple equations cannot in general quantitatively reproduce the MCP-PMTs behavior and detailed physical mechanisms, such as ion feedback and gain saturation effects, are required to be taken into account, these are still useful for basic considerations. Some remarks are made below:

- *BINP10s pulse shape*: We mention earlier that BINP10 exhibits a ringing-like signal shape (see, Fig. 2(b)); nevertheless, its pulse rise is fast enough to provide a time resolution of 35 ps. After the performance measurement reported above, we shortened the cable length between the MCP-PMT and the divider to reduce their inductances and changed the divider resistance ratio. Even though a small oscillating

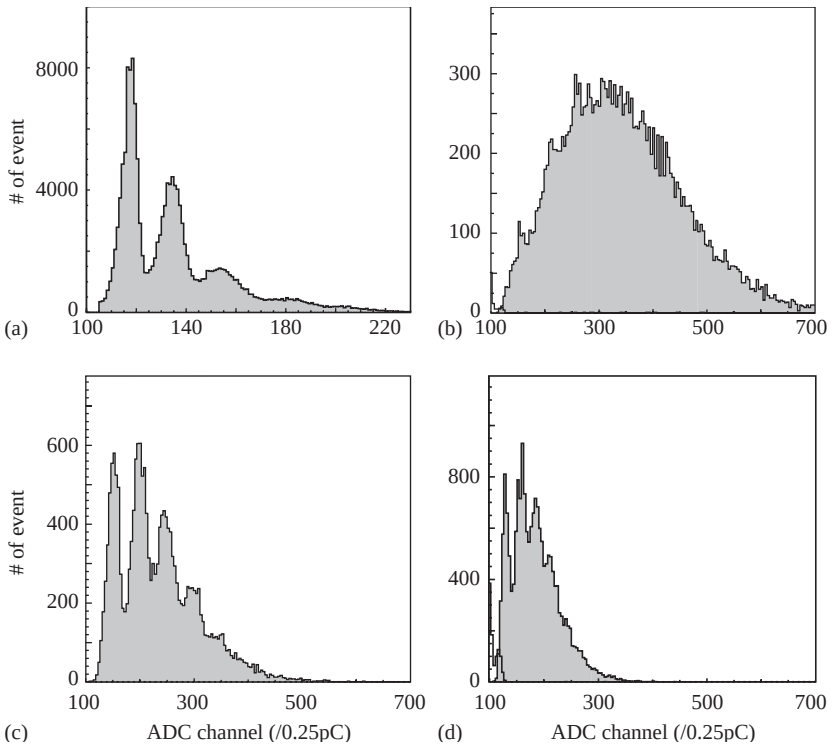

Fig. 11. ADC distributions for multi-photons irradiation under $B = 1.5$ T. (a) HPK6 at $\phi = 0°$, (b), (c) and (d) BINP10 at $\phi = 0°$, 15° and 30°, respectively.

component still remains, the pulse shape is very much improved, similar to that of HPK10. (see, Fig. 14). The timing properties are unchanged with this modification. We expect the signal to be better shaped with further optimization of the HV divider and readout electronic system.

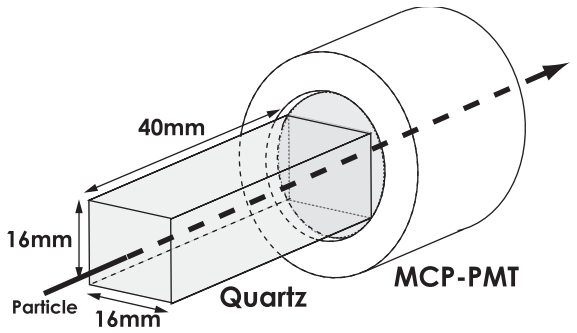

Fig. 12. Schematic drawing of the test TOF counter. HPK10 is used as the MCP-PMT.

- *Effective HV over MCP plates*: It is calculated by considering the divider resistance ratios (see, Table 1) on HV applied to the MCP-PMT. While HPK6, HPK10 and Burle25 function at the same effective HV range of 1.8–2.1 kV, the former PMT achieves a 10-times higher gain than those of the latter two. On the other hand, BINP10 is at the 2.4–2.8 kV range and obtains a similar gain to that of HPK6. When the G behavior of BINP10 is linearly extrapolated on a logarithmic scale to the 1.8–2.1 kV region, it would have a similar gain magnitude with HPK10 and Burle25. It is a suggested behavior by Eq. (1): All MCP-PMTs under no B-field should have the same gain, since there is no parameter to distinguish any specific MCP-PMT with a common α-ratio. It is therefore interesting to apply this rule to HPK10 and Burle25 operating at 2.4–2.8 kV, if it is operational; $\sigma_{TTS} \simeq 30$–40 ps would be attained.

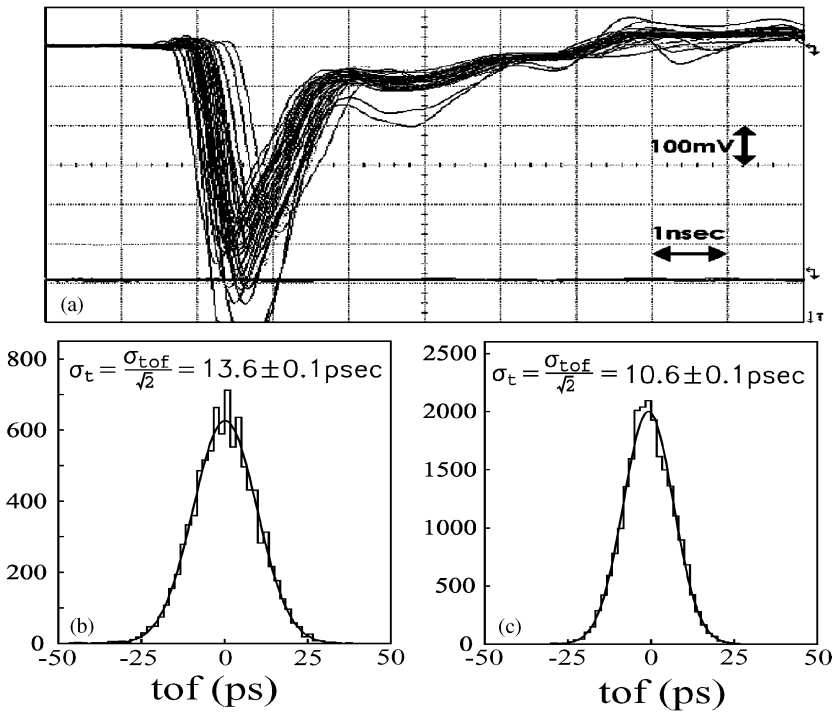

Fig. 13. (a) shows HPK10s output signal for 3 GeV/c pion beam; (b) and (c) are the distributions of the time difference between two test counters without and with a quartz radiator, respectively. Their resulting time resolutions of the single counter are obtained as $\sigma_t = \sigma_{tof}/\sqrt{2} = 13.6 \pm 0.1$ ps and 10.6 ± 0.1 ps.

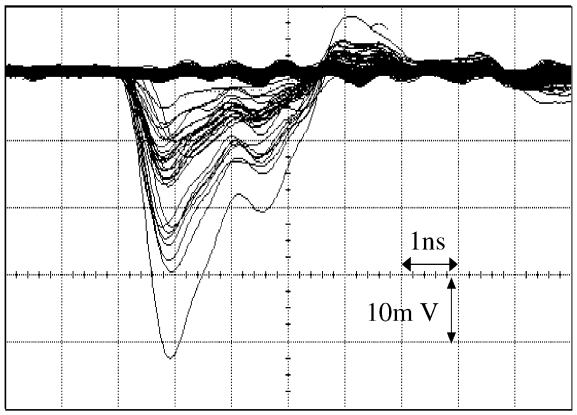

Fig. 14. Output pulses of BINP10, after shortening the cable length to the divider and changing the divider resistance ratio to 3.5:25:1.

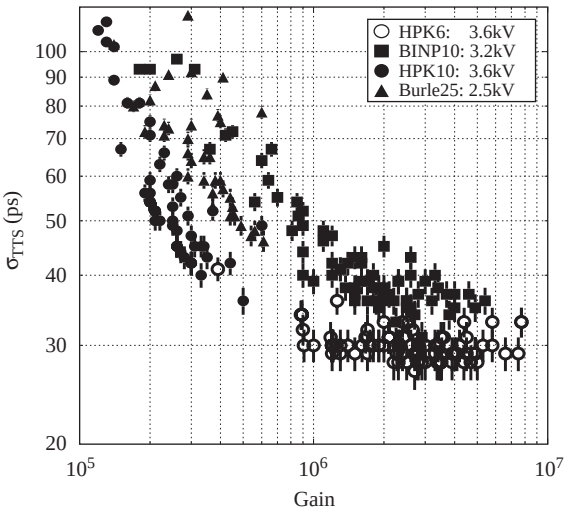

Fig. 15. G vs. σ_{TTS} for four MCP-PMTs under no B-field.

HKP6 does not follow this universal behavior: the small diameter of $D = 6\,\mu m$ causes some essential effect.

- *HV over photocathode-MCP*: This voltage is 1000 V for HPK6 and HPK10, 300 V for BINP10, and 200 V for Burle25 at their HV values of 3.6, 3.4, and 2.8 kV, respectively. The secondary emission factor ($\delta(V)$) has a maximum value around $eV_c \simeq 300$ eV. ($\delta(V)$ depends on the MCP material, but no specification is found for all MCP-PMTs. Therefore, we ignore the details of $\delta(V)$ and use the data in Ref. [6].) This voltage is well optimized for BINP10 and Burle25. On the other hand, HPK6 and HPK10 need higher voltages for photo-electrons to penetrate through the thin aluminum film for ion feedback prevention.
- σ_{TTS}: Figs. 10 and 15 show the σ_{TTS} vs. G relation for four MCP-PMTs, where the B-field strength and HV are not distinguished. All of the MCP-PMTs exhibit a rather linear relation in a $\log(G)$ vs. $\log(\sigma_{TTS})$ plot until the saturation phenomenon appears on σ_{TTS}.

  σ_{TTS} is saturated at 30 ps when $G \simeq 1 \times 10^6$ for HPK6, or 35 ps when $G \sim 2 \times 10^6$ for BINP10. Since the timing fluctuation of the electronics circuit is only ~ 10 ps, the resulted resolution (σ_{TTS}) is an intrinsic property of the MCP-PMTs.
- *Photon counting*: Under strong B-fields, the multiplicity of the photo-electrons is well identified in a linear relation to the ADC channel (see, Fig. 11), so that the photon counting method can be applicable with using the MCP-PMTs. It is presumed that individual photo-electrons are multiplied independently at each relevant region of the MCP plate, and that the resultant final secondary electrons of all photo-electrons are summed up at the anode.
- *MCP-PMT as a particle detector*: When a charged particle passes through the MCP plate, MCP-PMT alone functions as a detector, as reported in the last section for HPK10. There are two source materials: One is the photocathode window and the other is the MCP plate, itself. Although a similar number of photo-electrons are produced at both materials under straight beam injection, the timing of two processes differs as follows. The photo-electron from the photocathode needs ~ 100 ps to reach the front end of the MCP across a 1 mm-distance, while a relativistic particle passes across it by ~ 3 ps to produce secondary electrons. Nevertheless, these two cannot be distinguished with the MCP-PMTs time resolution.

Table 3
Resultant G and σ_{TTS} for four MCP-PMTs under $B = 0$ and 1.5 T (0.8 T for Burle25)

	HPK6	BINP10	HPK10	Burle25
G (0 T)	4×10^6	3×10^6	3×10^5	4×10^5
(1.5 T)	3×10^6	3×10^6	2×10^5	2×10^5
σ_{TTS} (0 T)	30 ps	30 ps	40 ps	60 ps
(1.5 T)	30 ps	35 ps	60 ps	100 ps

HKP10 provided $\sigma_t \sim 14$ ps at a beam test. It is a quite good resolution for TOF measurements, although the MCP-PMT surface size is small.

The photo-electrons from the former source cause essential timing and spacial spreads of the output signals. Therefore, a suppression of the former photo-electrons by removing the photocathode could possibly bring about a better timing resolution.

- *The TOF counter with* $\sigma_t < 10$ ps: The TOF counter tested here has a specific usage condition that an incident charged particle hits nearly normal to the counter, but it is not so peculiar.

  The intrinsic time resolution σ_0 of the TOF counter with HPK10 is inspected to be 6–7 ps, when $\sigma_t^2 = \sigma_{circuit}^2 + \sigma_0^2$ is supposed. To have a resolution σ_t better than 10 ps, a faster and more stable circuit system has to be prepared. When $\sigma_{circuit}$ is reduced to be a marginal component, the use of HPK6 or BINP10 would further improve σ_t, since their σ_{TTS} is about one half of HPK10s σ_{TTS}.

  To use of a thicker radiator, of course, also provides a better resolution.

The attained gain and time resolution (σ_{TTS}) for single photo-electrons are listed in Table 3. HPK6 and BINP10, especially, provide $\sigma_{TTS} \simeq 30$ and $\simeq 35$ ps, respectively, even under a 1.5 T magnetic field. Achieving such a high time resolution requires a high multiplication gain of a few-times 10^6; with such a high-gain condition the B-field influence on G and σ_{TTS} is very moderate and harmless.

Acknowledgements

We would like to thank Professors Y. Tihkonov, A. Bondar, G. Fedotovich, B. Shwartz, A. Onuchin, E. Kravechenko for their many valuable discussions and granting us the rights to own BINP10s. Special thanks go to Prof. B. Shwartz for reading this manuscript. We are also grateful to Mr. K. Yamauchi and H. Nishizawa of Hamamatsu Photonics K. K. for their useful advice and support in testing MCP-PMTs under the magnetic field. This work is supported by a Grant-in-Aid for Science Research on Priority Area (Mass Origin and Supersymmetry Physics) from the Ministry of Education, Culture, Sports, Science and Technology of Japan.

References

[1] V.V. Anashin, et al., Nucl. Instr. and Meth. A 357 (1995) 103;
H. Kichimi, et al., Nucl. Instr. and Meth. A 325 (1993) 451;
E. Morenzoni, et al., Nucl. Instr. and Meth. A 263 (1988) 397;
K. Oba, P. Rehak, IEEE Trans. Nucl. Sci. NS-28 (1981) 683;
J.L. Wiza, Nucl. Instr. and Meth. 162 (1979) 587;
G.W. Goodrich, W.C. Wiley, Rev. Sci. Instrum. 32 (1961) 846.

[2] M. Akatsu, et al., Nucl. Instr. and Meth. A 440 (2000) 124;
T. Ohshima, ICFA Instr. Bull. 20 (2000) 2;
T. Ohshima, Nucl. Instr. and Meth. A 453 (2000) 331;
M. Hirose, et al., Nucl. Instr. and Meth. A 460 (2001) 326;
S. Matsui, et al., Nucl. Instr. and Meth. A 463 (2001) 220;
T. Hokuue, et al., Nucl. Instr. and Meth. A 494 (2002) 436.

[3] Y. Enari, et al., Nucl. Instr. and Meth. A 494 (2002) 430;
M. Akatsu, et al., Nucl. Instr. and Meth. A 502 (2003) 133.

[4] Y. Katsuki, et al., Rev. Sci. Instr. 70 (1999) 3319.

[5] J. Adams, B.W. Manley, IEEE Trans. Nucl. Sci. NS-13 (1966) 88.

[6] A. Authinarayanan, R.W. Dudding, Adv. Electron. Electron Phys. 40A (1976) 167.